Title: Higher frequency of homologous chromosome pairing in human adult aortic endothelial cells

Running title: Chromosome pairing in aortic endothelial cells

Authors: Jemery Morales, Gabriel Quintero Plancarte, and Lisa Hua

Affiliations

Biology Department, Sonoma State University, Rohnert Park, CA 94928

Corresponding Author Email: hual@sonoma.edu

Contributions

J.M., and G.Q.P., performed experiments; J.M., G.Q. P., and L.L.H. conducted analysis; J.M., G.Q.P., and L.L.H. wrote the first draft of the manuscript. All authors read and approved the final manuscript.

Keywords

Antipairing, homologous chromosomes, human aortic endothelial cells, mitosis, nuclear organization

Word Count: 10,602

Abstract

During mitosis, pairing of homologous chromosomes can be detrimental and has been correlated with gene misregulation, chromosomal aberrations, and various pathological diseases. We previously demonstrated that homologous chromosomes are spatially segregated, or antipaired, in neonatal human endothelial cells at metaphase/anaphase, which may help prevent abnormal recombination. However, it is unclear if this antipairing persists in adult endothelial cells. To test whether the antipairing, or one homolog per nuclear hemisphere motif, is conserved in adult endothelial cells, we examined human aortic endothelial cells at metaphase. Using ImmunoFISH and high-resolution confocal microscopy to visualize the chromosomes and centrosomes, we found that small homologous chromosomes 13, 15, 17, 19, 21, 22, and the sex chromosomes, XY, exhibit a loss of spatial segregation in human adult aortic endothelial cells. In contrast, fewer adult endothelial cells showed a loss of segregation for the larger chromosomes 1, 4, and XX, suggesting a gradual decline in the fidelity of spatial segregation of homologous chromosomes. Notably, we observed a higher frequency of abnormal pairing in both small and large chromosomes in adult aortic endothelial cells as compared to neonatal umbilical vein endothelial cells. These findings suggest that mechanisms governing chromosome antipairing may decline with aortic endothelial cell age, leading to increased susceptibility to abnormal pairing and cardiovascular disease.

Introduction

Research has highlighted a significant link between chromosome organization and aging. [1-4] As endothelial cells (ECs) age, they exhibit decreased proliferative capacity, leading to senescence, impaired wound healing, and vascular repair.[5-10] Aging ECs may experience chromosomal abnormalities and mitotic dysfunction, resulting in errors during cell division and contributing to aneuploidy.[8,11-16] They are also more likely to enter a state of senescence, characterized by growth arrest and altered function, often triggered by oxidative stress and DNA damage.[5,7,8,17,18] Changes in expression of cell cycle regulators increase the likelihood of mitotic errors and further decline overall mitotic activity.[19,20] This decline in mitotic function and increased senescence contribute to cardiovascular dysfunction, a hallmark of aging,[5-8,21] making the reduction in mitotic activity in aging ECs a critical factor in cardiovascular aging.

Aged ECs exhibit various chromosome abnormalities that can lead to cellular dysfunction and age-related diseases.[20,22] These cells often show an abnormal number of chromosomes, disrupting normal functions and increasing cardiovascular disease risk.[20,22,23] For example, human aortic ECs derived from older patients show an increase in frequency aneuploidy (tetrasomy) in comparison to ECs derived from younger patients (18 months to 30 years old).[16] Structural abnormalities, such as deletions, duplications, inversions, and translocations, can result in gene misregulation.[24,25]

Changes in chromatin structure further alter gene expression and increase susceptibility to DNA damage, with aging associated with higher levels of damage due to oxidative stress.[2,26-31] Notably, the spatial arrangement of chromosomes within the cell may become disorganized in aged ECs, which can impact gene expression and overall cellular function. However, the specific changes in chromosome arrangement and non-random patterning in aged ECs remain unclear. These abnormalities reflect the genomic instability characteristic of aging, significantly affecting EC health and function.

Chromosomal organization is important for cell function, particularly during mitosis when a cell divides to produce two identical daughter cells and maintain the correct chromosome number across cell divisions.[31-35] Non-random chromosome organization may play a role in maintaining genomic stability. Research from our lab has shown that homologous chromosomes in neonatal human umbilical vein endothelial cells (HUVECs) are arranged on opposite sides of the centrosome axis during metaphase/early anaphase, resulting in a haploid set on either side.[36,37] This haploid set organization, or antipairing, pattern may minimize homologous chromosome pairing, indicating its importance in early development.

However, it is still unclear whether this antipairing pattern persists into adulthood. The loss of antipairing may increase the chances of homologous chromosome pairing, leading to mitotic recombination and potential genomic instability. This loss has been correlated to renal cancer and altered gene expression.[38,39] This finding suggests that abnormal somatic pairing and the loss of antipairing could be related to various human pathologies.[36,38,40] Despite this, there has been no thorough investigation into homologous chromosome organization in aged ECs, and a comprehensive analysis of this organization during mitosis is still lacking.

In this study, we employed 3D imaging to examine the organization of homologous chromosomes in adult human aortic endothelial cells (HAECs) sourced from individuals, both female and male, aged from 21 years to 68 years, and cultured at low passage numbers. Using immunofluorescence and DNA fluorescence *in situ* hybridization (ImmunoFISH) and high-resolution confocal microscopy, we analyzed the positions of homologous chromosomes in HAECs to determine whether the spatial segregation of homologous chromosomes, or antipairing, persists in adult aortic endothelial cells. Our findings reveal that mitotic antipairing is lost in adult aortic ECs. Small chromosomes 13, 15, 17, 19, 21, 22, and Y lose their spatial segregation in HAECs, while fewer HAECs showed loss of segregation for the larger chromosomes 1, 4, and X. This suggests a gradual decline in the fidelity of spatial segregation

of homologous and sex chromosomes. Both small and large chromosomes exhibit a higher frequency of abnormal homologous pairing in adult HAECs compared to neonatal HUVECs, with smaller chromosomes, including the acrocentric ones, showing a greater frequency of abnormal pairing than larger chromosomes in adult HAECs. There are at least two potential causes for this higher pairing frequency and the loss of antiparing: one would be an age-dependent change, and the other would be an aorta-specific mechanism to enhance the loss of antipairing. Overall, our data indicate that the mechanisms governing chromosome antipairing organization declines, or loses fidelity, in aged aortic ECs.

Materials and Methods

Cell culture

Primary human umbilical vein endothelial cells (HUVECs, ATCC: Cat. No. PSC-100-013, Lot # 70032758 and 81006213) were cultured as previously described.[36,37] Human aortic endothelial cells (HAECs), (Lonza: Cat. No. CC-2535, Lot #: 0000430739, 22TL13791, 0000351486, 0000337673, 21TL076036, 22TL073027) were derived from individual human donors (21 year old male, 36 year old female, 50 year old male, two 50 year old females, and 68 year old male) and were fixed at low passage (<7). MCDB-131 (Cat No. 10372-019), 1% Glutamax (Cat No. 35050-061), 1% Pen-strep (Cat No. 15140-122), and 2% Large vessel endothelial supplement (Cat No. A14608-01) were used for cell growth. Cells were grown on a 10 cm dish until reaching a confluency of 70-80% and then transferred onto a 15 cm plate containing 2 well, 8 mm well diameter PTFE glass slides (Electron Microscopy Sciences, Cat. No. 63416-08), which were flamed/UV sterilized.

Immunofluorescence and Chromosome painting

HUVECs and HAECs were grown on PTFE glass slides to 80-90% confluence. The slides were fixed with 4% paraformaldehyde. After, the slides were stored in 70% ethanol for at least 24 hours.

Immunofluorescence

Slides were washed three times in 4ºC 1x Phosphate Buffered Saline (PBS) on ice before undergoing heat-induced antigen retrieval for 10 minutes in a sodium citrate buffer solution (10 mM sodium citrate, 0.05% Tween-20, pH 6.0) in a steamer. Slides were then washed in a permeabilization buffer (0.25% Triton X-100 in 1x PBS) for 10 minutes followed by three 1x PBS washes at room temperature (RT). A blocking buffer (10% goat serum, 0.1% Tween-20 in 1x PBS) was then applied for 30 minutes at RT. Slides were incubated with a primary antibody to γ-tubulin [1:1000, abcam: Rabbit Anti-γ-tubulin antibody (ab11317)] diluted in 10% goat serum in 1x PBS with 0.1% Tween-20. Parafilm was used to cover slides. Slides were then incubated at 4°C in a humidified chamber overnight. The following day, the slides were washed three times with 1x PBS. Incubation of a secondary antibody [1:500, abcam: Goat Anti-Rabbit IgG H&L (Alexa Fluor® 647) (ab150079)] (in 1% BSA in 1x PBS with 0.1% Tween-20) was applied to slides, covered in Parafilm, and incubated in the dark for 1 hour at RT. Slides were then washed twice with 1x PBS, and processed with DNA counterstain DAPI (Invitrogen: D1306) for immunofluorescence. The slides were washed twice in 1x PBS. After, Antifade (Invitrogen: Cat. No. P36930) was applied with a 24X60 mm coverslip (Corning: Cat. No. 2980-246, #1.5) and sealed with nail polish. The slides were stored at 4ºC until using the confocal microscope.

Immunofluorescence and Chromosome painting

If continuing on for chromosome painting, before processing with the DNA counterstain steps listed above, the slides were incubated with an EGS crosslinker solution (25% DMSO, 0.375% Tween-20, 25mM EGS (Thermo Scientific: Cat. No. 21565) in 1x PBS) for 10 minutes in

the dark at RT. Slides were washed twice with 1x PBS. Whole Chromosome Paints for chromosomes 1, 4, 13, 15, 17, 19, 21, 22, XX, and Y in Aqua, Texas red, or FITC (Applied Spectral Imaging) were used to visualize individual chromosomes in metaphase cells. The probes were preheated on an 80ºC heat block for 10 minutes. Then, the probes were incubated at 37ºC for 1 hour. The slides were washed with a buffer containing saline-sodium citrate (2x SSC) (Cat. No. 15557-044). After, the slides were submerged in 0.1 N HCl for 5 minutes at RT. Then, the slides were washed with 1x PBS, three times for 5 minutes, followed by a series of chilled ethanol washes on ice. The slides were placed in a denaturation solution (20X SSC, formamide, deionized water) for 7 minutes at 80ºC followed by a second series of cold ethanol washes on ice. The slides were incubated with probes on a slide warmer. An 8 mm (World Precision Instruments: Cat. No. 052041) and 12 mm coverslip (Electron Microscopy Sciences: Cat. No. 72290-04) were stacked in subsequent order on the wells, and sealed with rubber cement. The slides were incubated in a moisturizing container containing formamide and deionized water, overnight at 37ºC. The following day, the slides were washed in a post-hybridization buffer (1% Tween-20, 10% 20x SSC in deionized water) at 42ºC for 10 minutes, three times. Slides were then incubated with a DNA counterstain (DAPI, Hoechst, SYTOX, or TO-PRO-3, Invitrogen: Cat. No. D1306, H1399, S11380, T3605). The slides were washed twice in 1x PBS. After, Antifade was applied with a 12 mm coverslip and sealed with nail polish. The slides were stored at 4ºC until using the confocal microscope.

Confocal microscopy

Fixed cells were imaged using a laser scanning confocal microscope (Leica: TCS SPE, DM2500) using a 63x/1.3NA oil immersion objective with a digital zoom of 1.5x to visualize individual cells. The z-stacks were acquired sequentially in a four-channel mode; z-stacks were captured using a frame size of 1,024x1,024 pixels and processed with Leica Application Suite X software (Version: 3.5.2.18963).

3D reconstruction and overlay, distance and angular orientation measurements of homologous chromosomes

Confocal optical sections were reconstructed in a 3D software, Imaris (Bitplane: 9.8.2). Three-dimensional overlay generation of homologous chromosomes in multiple fixed metaphase HUVECs and HAECs was performed as previously described (Hua and Mikawa 2018). Calculations and plot generation for 2D positional analysis, as well as 3D distance and angular measurements between homologous chromosomes in fixed HUVECs and HAECs, were performed as previously described.[36] Multiple pairs of homologous chromosomes were visualized by creating the cellular axis that was previously defined by Hua and Mikawa.[36] The x, y, and z axes were set an origin of 0,0,0 to define each nuclear hemisphere across the x-axis (centrosome axis), and to analyze how each pair of homologous chromosomes spatially position themselves in relation to the centrosome axis. The center of mass of the centrosomes by γ-tubulin immunofluorescence staining defined the x-axis and was used for alignment of metaphase cells. The position of each homolog was analyzed. The position of each pair of homologous chromosomes was normalized in every mitotic cell with regards to the DNA counterstain similar to Hua and Mikawa.[36]

Statistical analysis

We tested for nonrandom distributions of autosomes and sex chromosomes across the two nuclear hemispheres using a binomial distribution test.[41] Pairing was defined as occurring in cells where homologs had a distance and angular orientation difference of 0. Contingency table analysis or logistic regression was used to assess the effect of explanatory factors on the probability of pairing. Statistical analysis was completed using the statistical analysis software, JMP Pro 17 (SAS Institute, Raleigh, NC)).

Data Visualization

All figures were generated using Adobe Photoshop (Version 26.3.0). Bar graphs depicting pairing frequencies of chromosomes between HUVECs and HAECs were generated with Graphpad Prism 10 (Version 10.3.1 (464)).

Rotational video of both single whole chromosome painting and 3D overlays for HUVECs and HAECs were generated using the video editing software, Adobe Premiere Pro (Version 25.0.0, Build 61). To show side-by-side comparison of chromosome positioning of both HUVECs and HAECs, each cell was repositioned and resized using the position tool for both X and Y, and the scale function within the properties tab. The text was implemented in the video using the type tool within the tools tab and the corresponding text colors were changed within the properties tab. Video was exported and used the preset: Match Source - Adaptive High Bitrate, Format of H.264 and recorded at 24 fps.

Results

Spatial segregation is maintained for small chromosomes 17 and 19 in neonatal human umbilical vein endothelial cells (HUVECs) at metaphase

Previously, it was found that a pair of homologous chromosomes reside on opposite sides of the centrosome, or nuclear division axis, in human neonatal cells at metaphase/early anaphase.[36] This one homolog on either side of the centrosome axis, or antipairing organization, was conserved for all chromosomes in the human karyotype of HUVECs at early anaphase.[36] To confirm that antipairing is present at metaphase, individual chromosomes were visualized in HUVECs (Fig. 1 A). A coordinate axis with a chromosome paint approach was performed as previously described,[36] in addition to ImmunoFISH to simultaneously visualize the centrosome axis (Supplemental Fig. 2 A-A”’). HUVECs are polarized cells with an apical and basal domain, which aided in establishment of an axial coordinate system.[36,42]

The nuclear hemispheres were previously defined by Hua and Mikawa (2018)[36] as the following: x-axis is the line that crosses the centrosomes, z-axis is the laser line, and y-axis is perpendicular to both the x- and z-axes at metaphase/anaphase (Fig. 1 A, Supplemental Fig. 2 A'-A"'). To evaluate the frequency of homologous pairing, we measured the minimal distance and angular orientation between each homologous pair as previously described[36] (Fig. 1 B). Pairing is defined as having a 0 μm distance and a 0º vector angle between a pair of homologous chromosomes (Fig. 1 B).

To determine whether the homologous chromosomes were segregated at metaphase, we performed ImmunoFISH to combine immunolabeling using a γ-tubulin antibody to visualize the centrosomes,[43] DNA FISH/Whole Chromosome Paint (WCP) to visualize chromosomes, and a DNA counterstain (Fig. 1 C, G, K, O). We then determined if a pair of homologous chromosomes resided on the same side or opposite side of the centrosome axis (Supplemental Fig. 2 A'-A"'). ImmunoFISH/WCP was carried out for pooled samples of neonatal HUVECs (n=20 individuals, Table 1). Chromosomes 17 and 19 were selected based on differences in length/size of base pairs.[44] Metaphase cells were identified based on the highly condensed chromosomes aligned in the middle of the cell, with centrosomes positioned at the opposite poles.[45] Segregation of homologous chromosomes 17 and 19 was observed in a HUVEC at metaphase (Fig. 1 C, G).

To determine whether segregation of homologous chromosomes 17 and 19 occurred in multiple HUVECs, we created a 3D overlay as previously described.[36] (Supplemental Fig. 2 for chromosome 19). The centrosome or x-axis, defined by positive γ-tubulin staining, or the center of DNA mass for each cell were used to establish an origin point (0,0,0) for alignment in the 3D overlay analysis (Supplemental Fig. 2 A'). The position of individual chromosomes was determined by identifying the center of mass of the chromosome paint signal (Supplemental Fig. 2 A"-A"'). The 3D overlay of chromosomes 17 and 19 at metaphase demonstrated that multiple HUVECs displayed segregation of homologous chromosomes 17 and 19 along the centrosome

axis (Fig. 1 D, H, Supplemental Fig. 2 B). Mapping of individual positions of the homologous chromosomes 17 and 19 in each HUVEC revealed that one homolog consistently positioned itself on each side of the centrosome axis (Fig. 1 E, I segregation in n=12/12 cells for chromosome 17; segregation in n=33/35 cells for chromosome 19). In no case did we see homologous chromosomes 17 or 19 exhibit pairing at 0 μm distance or 0° angular orientation relative to its partner similar to our previous study[36] (Fig. 1 F, J). This data demonstrated that chromosomes 17 and 19 were consistently antipaired in HUVECs at metaphase. Similar to our previous reports at anaphase, these data indicate that the homologous chromosomes 17 and 19 are organized in a non-random, antipaired configuration.[36]

Homologous chromosome segregation is lost in small chromosomes 17 and 19 in adult HAECs

To investigate whether the antipairing pattern is present in adult aortic endothelial cells (HAECs), we performed ImmunoFISH/WCP for chromosomes 17 and 19 in single donor-derived HAECs (Table 1). Analyzing individual donor samples offer insights into whether this pattern is lost or conserved in adult aortic endothelial cells (ECs) across the general population. If the antipairing pattern is absent in multiple patients, it may suggest that this loss is consistent across the adult aortic EC population. On the other hand, if the antipairing pattern is lost in some patients but still present in others, it could indicate that the presence or absence is specific to individual patients.

HAECs are typically sourced from individual patients. Therefore, to investigate whether this pattern is present across multiple patients, we analyzed individual HAECs at metaphase (Table 1, n=4 patients for chromosome 17, n=4 patients for chromosome 19). The five patients included a 36-year-old female, two 50-year-old females, a 50-year-old male, and a 68-year-old male (Table 1). We selected individuals from different age groups and sexes to determine if the antipairing pattern is preserved among adult aortic ECs.

To determine whether small chromosomes maintain the spatial segregation of homologs in adult HAECs, we analyzed chromosomes 17 and 19 using ImmunoFISH/WCP. We found that both chromosomes 17 and 19 lose the pattern of one homolog per nuclear hemisphere in HAECs derived from five patients (Fig. 1 K-R n=82 cells for chromosome 17; n=38 cells for chromosome 19, Table 1). Quantification analysis revealed average distances of 1.66 ± 1.39 μm SD, 2.02 ± 1.79 μm SD and angular orientations of 101.0° ± 51.2° SD, 93.8° ± 55.8° SD for homologous chromosomes 17 and 19, respectively (Fig. 1 N, R).

Notably, chromosome 17 was found to be abnormally paired in 12 out of 82 cells in three patients, the 36-year-old and 50-year-old females, and 68-year-old male (Fig. 1 N, Table 1). The 50-year-old female and 68-year-old male also displayed pairing of chromosome 19 in four out of 38 cells (Fig. 1 R). Together, these data show that small chromosomes 17 and 19 lose the spatial segregation and exhibit an increase of 13% abnormal pairing (16 out of 120 cells) in adult HAECs as compared to 0% of neonatal HUVECs (0 out of 47 cells) (Fig. 1 S).

However, both chromosomes 17 and 19 are small non-acrocentric chromosomes. To further investigate whether other small chromosomes that are acrocentric also lose the spatial segregation,[46] we next mapped the position of small acrocentric chromosomes to determine if the loss of spatial segregation is shared broadly among the human karyotype.

Homologous segregation is lost in acrocentric chromosomes 13, 15, 21, and 22 in adult HAECs

Acrocentric chromosomes including 13, 14, 15, 21, 22, and Y, are small chromosomes that have the centromere located near one end of the chromosome, and contain the nucleolus organizing region.[47] To test whether small acrocentric chromosomes also lose the one homolog pattern in adult HAECs, we selected acrocentric chromosomes 13, 15, 21, and 22 to analyze.

Our previous study has shown that one homolog per nuclear hemisphere motif is a conserved pattern for acrocentric chromosomes in neonatal HUVECs.[36] Three-dimensional overlays of neonatal HUVECs showed segregation of chromosomes 13, 15, 21, and 22 at metaphase (Fig. 2 A-L, segregation in n=33/33 cells for chromosome 13; segregation in n=33/41 for chromosome 15; segregation in n=27/32, for chromosome 21; segregation in n=18/22 for chromosome 22; Supplemental Video 1). Pairing of homologous chromosome 21 was observed in one out of 32 cells (Fig. 2 I). These data confirm the homologous segregation of acrocentric chromosomes 13, 15, 21, and 22 in HUVECs with almost no pairing.

In contrast, 3D overlays of adult HAECs for chromosome 13, 15, 21, and 22 demonstrated a loss of the one homolog per nuclear hemisphere motif (Fig. 2 M-Y, n=47 cells for chromosome 13, n=50 cells for chromosome 15, n=51 cells for chromosome 21, n=52 cells for chromosome 22, respectively). Abnormal pairing of the acrocentric chromosomes 13, 15, 21 and 22 was observed in 4 out of 4 patients, 3 out of 3 patients, 3 out of 4 patients, and 1 out of 6 patients, respectively (Fig. 2 M-Y). Together, these data show that small acrocentric chromosomes 13, 15, 21, and 22 lose the spatial segregation and exhibit an increase of 19.50% of abnormal pairing (39 out of 200 cells) in adult HAECs as compared to 0.78% of neonatal HUVECs (1 out of 128 cells) (Fig. 2 Z).

The one homolog per nuclear hemisphere motif along the centrosome axis was lost for the acrocentric chromosomes 13, 15, 21 and 22 in six adult patients. These data show that the small chromosomes, both non-acrocentric and acrocentric, lose the one homolog per nuclear hemisphere motif and have an increased frequency of homologous pairing. To rule out the possibility that a loss of antipairing and an increase in abnormal pairing events may not be limited to small chromosomes only, we next decided to investigate positioning of large chromosomes.

Fewer adult HAECs show loss of segregation for the larger chromosomes 1 and 4

To test whether large chromosomes also lose the spatial segregation of homologous chromosomes as observed in non-acrocentric and acrocentric adult HAECs, we mapped the positions of chromosomes 1 and 4 using ImmunoFISH/WCP.

Compared to chromosomes 1 and 4 in HUVECs at metaphase, which showed consistent segregation along the centrosome axis (Fig. 3 A-F; n=29/31 cells for chromosome 1, n=26/28 cells for chromosome 4), fewer HAECs displayed segregation for the larger chromosomes 1 and 4. However, a higher number of HAECs across multiple patients (n=6 patients for chromosome 1, n=5 patients for chromosome 4) lost segregation of the one homolog per nuclear hemisphere motif (Fig. 3 H, K; segregation in n=48/60 cells for chromosome 1; segregation in n=35/50 cells for chromosome 4, Table 1), suggesting a gradual decline in the fidelity of spatial segregation of homologous chromosomes.

Notably, pairing of homologous chromosomes 1 and 4 was observed in single HAECs of both the 21-year-old and 50-year-old males (Fig. 3 I, L). Abnormal pairing of chromosomes 1 and 4 were present for different cells. Two additional cells of the 50-year-old female also showed chromosome 4 pairing (Fig. 3 L). In contrast, there was no abnormal pairing for chromosomes 1 and 4 in HUVECs (Fig. 3 C, F). These data reveal that large chromosomes 1 (3.3%) and 4 (8.0%) in adult HAECs show a loss of spatial segregation, with a combined 5% of cells (6 out of 110) displaying abnormal pairing. This contrasts with neonatal HUVECs, where no abnormal pairing was observed (0 of 59 cells) (Fig. 3 M).

Abnormal pairing is observed less frequently in larger chromosomes as compared to smaller chromosomes in HAECs. Chromosomes 1 and 4, which are larger, show only a minor loss in spatial segregation (5%, 6 out of 110), while acrocentric chromosomes 13, 15, 21, and 22 exhibit a more significant loss of 17.19% (55 out of 320) in HAECs (Fig. 2 Z). These findings

suggest small chromosomes lose their spatial segregation in HAECs, while fewer HAECs show loss of segregation for the larger chromosomes 1 and 4. This indicates a gradual loss of fidelity in the spatial segregation of homologous chromosomes.

Abnormal pairing was also observed in smaller chromosomes, including the acrocentric chromosomes, 13, 15, 17, 19, 21, and 22 in 61 out of 430 cells (14.18%), indicating that the mitotic antipairing pattern is lost in adult aortic ECs (Fig. 1 S; Fig 2 Z; Fig. 3 M). Collectively, both large and small chromosomes have a higher frequency of abnormal pairing in adult aortic ECs as compared to neonatal HUVECs. Next, we aimed to investigate whether the sex chromosomes also exhibit a loss of spatial segregation in adult HAECs.

Fewer female adult HAECs exhibit loss of X chromosome spatial segregation and abnormal pairing, while in male adult HAECs, the XY sex chromosomes lose segregation but do not pair

To test whether the X chromosomes in females or XY chromosomes in males lose their segregation pattern in adult HAECs, we performed ImmunoFISH/WCP (Fig. 4 G-L). HUVECs were reported to show spatial segregation of the XX and XY sex chromosomes along the centrosome axis in female and male neonatal HUVECs supporting that the mitotic antipairing organization was sex-type independent.[36] The X and XY chromosomes in female and male HUVECs showed segregation (Fig. 4 A-F, segregation in n=19/19 cells for chromosome XX in females, segregation in n=13/16 cells for XY in males, n=20 patients, Table 1) consistent with our previous results.[36] In no case did we see homologous chromosomes X or XY exhibit pairing at 0 μm distance or 0° angular orientation relative to its partner (Fig. 4 A-F).

However, fewer adult HAECs from three female patients showed a loss of X chromosome segregation, along with an increase in abnormal pairing (Fig. 4 G-I, segregation in n=67/86 cells, Table 1). Four cells from both the 36-year-old and the 50-year-old female patients

showed abnormal pairing of 4.7% (n=4/86 cells). These data suggest that homologous chromosomes X, as well as the large chromosomes 1 and 4, all exhibit a similar frequency of 5% abnormal pairing in adult HAECs.

Acrocentric chromosomes in adult HAECs are shown to be abnormally paired and lose their segregation (Fig. 2). The Y chromosome is also an acrocentric chromosome.[48] To test whether the XY chromosomes also lose the one sex chromosome per nuclear hemisphere motif in adult HAECs, we completed ImmunoFISH/WCP of three individual male HAECs (Fig. 4 J, Table 1). We found that XY chromosomes lose the one sex chromosome per hemisphere motif (Fig. 4 J-L, n=44 cells). However, pairing of XY was not observed in contrast to the abnormal pairing observed in XX in female adult HAECs (Fig. 4 I, L). These data suggest that there may be a greater affinity for similar sequences like the X chromosomes or homologous chromosomes to be abnormally paired as compared to XY chromosomes. The homologous chromosomes that lose the one homolog per hemisphere motif show a higher frequency of pairing in HAECs. The XY have different sequence homology and showed no pairing (Fig. 4 L, M).

Taken together, the X chromosomes show an increased frequency of abnormal pairing in three female patients, while the XY chromosomes do not exhibit abnormal pairing, yet they lose their segregation in three male patients. In summary, our data show that the sex chromosomes lose the spatial segregation pattern in adult aortic ECs.

Discussion

A proposed function of the antipairing organization is to minimize abnormal homologous pairing and recombination, and thus provide genomic stability with fidelity throughout multiple cell cycles. It was found that neonatal HUVECs display spatial segregation of homologous chromosomes for the human karyotype during metaphase/early anaphase.[36] Here, we find that

the spatial segregation of homologous chromosomes is lost for small chromosomes, and the XY sex chromosomes in adult aortic ECs. While fewer HAECs showed a loss of spatial segregation of the large chromosomes 1, 4, and X in females. Our data suggest the underlying mechanisms of homologous segregation differentially impacts chromosomes of different sizes (Fig. 5 A, X^2 (9, n=559) = 39.2, for all chromosomes individually, X^2 (2, n= 559) = 25.4, for chromosomes based on sizing). Additionally, when comparing acrocentric chromosomes to non-acrocentric chromosomes, we observed a higher frequency of pairing in acrocentric chromosomes (X^2 (1, n=559) = 7.54, p=0.0060).

There is a tendency for smaller chromosomes to localize along the centrosome axis or in the interior of the metaphase plate as compared to larger chromosomes.[49-52] One potential mechanism is that homologous chromosomes align to a cue along the centrosome axis. We have recently found a pattern of low centromeric staining using both DNA and protein markers along the centrosome axis in HUVECs that may act as a cue for chromosome alignment.[37] One possibility is the loss of the cue, a region of low centromeric components along the centrosome axis, which may initially affect the smaller chromosomes in proximity. Therefore, a differential loss of the spatial segregation would be observed for chromosomes of different sizes. It would be fruitful to determine whether this low centromeric staining pattern is lost in adult aortic ECs.

It is proposed that the loss of the antipairing organization can lead to a higher chance of pairing of somatic homologous chromosomes, and mitotic recombination, due to the close proximity of the homologs.[36] The loss of segregation leads to an increased frequency of abnormal pairing observed for chromosomes 1, 4, 13, 15, 17, 19, 21, 22, X with the exception of XY sex chromosomes in adult HAECs. These findings suggest that, after birth, there is an increased susceptibility to a loss of nuclear organization, which may lead to greater genome instability (Fig. 5 B, C). However, adult aortic ECs are less proliferative than neonatal HUVECs, so genomic instability may have a lesser impact, as fewer cellular divisions occur.

There have been previous studies reporting the loss of chromosomes, in particular small chromosomes, with age or passage number in cultured ECs, and hematological malignancies/disorders.[16,53-66] For example, *in vitro* populations of cultured human corneal EC is found to have an increase in frequency of aneuploidy with both age and passage number.[62,66]

The XY sex chromosomes lose the segregation pattern, yet they do not display increased pairing events (Fig. 4 J-L). The XY sex chromosomes have minimal sequence homology, except for the PAR1/2 regions, and display independent mechanisms of pairing in specific regions of each chromosome.[67] The minimal homology and independent pairing mechanisms of XY chromosomes could contribute to their susceptibility to loss in aged cells, as seen with an increase of whole chromosome Y loss in various tissues.[53- 56, 59-62, 68-70]

Abnormal karyotypes that are sex-specific, associates with the Y chromosome in hematopoietic and blood cells.[69] The Y chromosome exhibit distinct segregation and stability patterns both during cellular processes in HUVECs, and in the context of aging.[16] These studies suggest chromosome characteristics may be unique to the Y chromosome. This variability in both pairing mechanisms and chromosomal loss could provide insights into how sex chromosomes behave differently from autosomes in both developmental and aging processes. The possibility that the unique features of the Y chromosome—such as its limited sequence homology and independent mechanisms of pairing—might make it more prone to alterations in specific cellular contexts, particularly as cells age.

Due to the challenges in culturing human adult aortic ECs, we were only able to analyze samples from six adult patients: One male each aged 21, 50, and 68, and one female aged 36, along with two females aged 50. As a result, we cannot exclude the possibility that these individual cases may not reflect the broader population for chromosome organization.[71] For instance, the aortic ECs samples were collected from patients undergoing surgery for hypertension, which could potentially influence endothelial cell pathogenesis and chromosome organization. Additional data is necessary to draw more reliable conclusions.

We observed abnormal pairing of homologous chromosomes for all six patients, rather than only a few. This suggests the loss of antipairing is conserved in adult aortic ECs (Fig. 5 C). Whether the loss of antipairing in adult HAECs increases with age, and is associated with sex still remains elusive. Our study analyzed a subset of individuals across different age groups, which limited statistical analysis of age, and age with sex determinants. Nonetheless, graphical data suggests an age-dependent loss of spatial segregation of homologous chromosomes throughout adulthood (Fig. 5 B). Future studies are required to determine if the antipairing mechanism is lost in additional adult patients at various age groups. Using mouse models would also be valuable to more accurately study the aging of aortic ECs, reducing variability across samples, and allowing for a direct assessment of how aging affects chromosome organization.

There are at least two potential causes for the higher pairing frequency or loss of antipairing: one could be an age-dependent change, while the other may involve an aorta-specific mechanism that enhances the loss of antipairing. In this study, we focused on adult aortic EC populations. It would be advantageous to analyze different primary human adult EC lines to determine if the loss of antipairing pattern is endothelial cell-type dependent. In addition, our study only analyzes a subpopulation of chromosomes: 1, 4, 13, 15, 17, 19, 21, 22, XX, and XY. It would be beneficial to determine if other autosomes maintain or lose the antipairing organization in adult aortic ECs.

Importantly, the spatial arrangement of chromosomes within the cell can become disordered in adult aortic ECs, potentially affecting gene expression and overall cellular function. Our findings offer a better understanding of the mitotic antipairing pattern observed in human neonatal ECs, which may be lost with age. This loss of higher-order chromosome organization highlights its critical role in maintaining genomic stability in human cells.

Acknowledgements

I would like to express my heartfelt gratitude to my parents, Adolfo Morales and Silvia Cienfuegos, for their unwavering love and support throughout this journey. To my brothers, Adolfo and Alexis, thank you for your encouragement and understanding. I am also deeply grateful to my family friend, Alfonso Ventura, for his invaluable support. Your presence and guidance have been instrumental in the completion of this thesis. Thank you Drs. Takashi Mikawa and Joseph Lin for review and discussion of the manuscript, Dr. Daniel Crocker for support and discussion on statistical analysis, and Hua lab members for their guidance, feedback, and support. L.L.H dedicates this work to the memory of her daughter, Josephine Jereb. Part of this work is incorporated into a Master's thesis (J.M.).

Funding

This work was supported in part by National Science Foundation (NSF RUI Award #2027746 to L.L.H.), National Institutes of Health (NIH) (NIGMS Award #R16GM153517-01 to L.L.H), California State University Program for Education and Research in Biotechnology (CSUPERB New Investigator Grant to L.L.H.), Koret Foundation/ORSP grant (to G.Q.P, J.M, and L.L.H), and SSU start up funds (to L.L.H.).

Statements and Declarations

The authors declare no competing interests.

References

1. Chandra, T., & Kirschner, K. (2016). Chromosome organisation during ageing and senescence. *Current opinion in cell biology*, *40*, 161–167. https://doi.org/10.1016/j.ceb.2016.03.020

2. Liu, Z., Belmonte, J. C. I., Zhang, W., Qu, J., & Liu, G. H. (2022). Deciphering aging at three-dimensional genomic resolution. *Cell insight*, *1*(3), 100034. https://doi.org/10.1016/j.cellin.2022.100034

3. Guarente L. (1996). Do changes in chromosomes cause aging?. *Cell*, *86*(1), 9–12. https://doi.org/10.1016/s0092-8674(00)80072-0

4. Criscione, S. W., De Cecco, M., Siranosian, B., Zhang, Y., Kreiling, J. A., Sedivy, J. M., & Neretti, N. (2016). Reorganization of chromosome architecture in replicative cellular senescence. Science Advances, 2, e1500882. https://doi.org/10.1126/sciadv.1500882

5. Ting, K. K., Coleman, P., Zhao, Y., Vadas, M. A., & Gamble, J. R. (2021). The aging endothelium. *Vascular biology (Bristol, England)*, *3*(1), R35–R47. https://doi.org/10.1530/VB-20-0013

6. Bloom, S. I., Islam, M. T., Lesniewski, L. A., & Donato, A. J. (2023). Mechanisms and consequences of endothelial cell senescence. *Nature reviews. Cardiology*, *20*(1), 38–51. https://doi.org/10.1038/s41569-022-00739-0

7. Jia, G., Aroor, A. R., Jia, C., & Sowers, J. R. (2019). Endothelial cell senescence in aging-related vascular dysfunction. *Biochimica et Biophysica Acta (BBA)-Molecular Basis of Disease*, *1865*(7), 1802-1809. https://doi.org/10.1016/j.bbadis.2018.08.008

8. Guo, J., Huang, X., Dou, L., Yan, M., Shen, T., Tang, W., & Li, J. (2022). Aging and aging-related diseases: from molecular mechanisms to interventions and treatments. *Signal Transduction and Targeted Therapy*, *7*(1), 391. https://doi.org/10.1038/s41392-022-01251-0

9. Shabanian, K., Shabanian, T., Karsai, G., Pontiggia, L., Paneni, F., Ruschitzka, F., Beer, J. H., & Saeedi Saravi, S. S. (2024). AQP1 differentially orchestrates endothelial cell senescence. *Redox biology*, *76*, 103317. https://doi.org/10.1016/j.redox.2024.103317

10. Rippe, C., Blimline, M., Magerko, K. A., Lawson, B. R., LaRocca, T. J., Donato, A. J., & Seals, D. R. (2012). MicroRNA changes in human arterial endothelial cells with senescence: relation to apoptosis, eNOS and inflammation. *Experimental gerontology*, *47*(1), 45–51. https://doi.org/10.1016/j.exger.2011.10.004

11. Potapova, T., & Gorbsky, G. J. (2017). The Consequences of Chromosome Segregation Errors in Mitosis and Meiosis. *Biology*, *6*(1), 12. https://doi.org/10.3390/biology6010012

12. López-Otín, C., Blasco, M. A., Partridge, L., Serrano, M., & Kroemer, G. (2013). The hallmarks of aging. *Cell*, *153*(6), 1194–1217. https://doi.org/10.1016/j.cell.2013.05.039

13. Macedo, J. C., Vaz, S., & Logarinho, E. (2017). Mitotic Dysfunction Associated with Aging Hallmarks. *Advances in experimental medicine and biology*, *1002*, 153–188. https://doi.org/10.1007/978-3-319-57127-0_7

14. Lezhava T. (2001). Chromosome and aging: genetic conception of aging. *Biogerontology*, *2*(4), 253–260. https://doi.org/10.1023/a:1013266411263

15. Guttenbach, M., Koschorz, B., Bernthaler, U., Grimm, T., & Schmid, M. (1995). Sex chromosome loss and aging: in situ hybridization studies on human interphase nuclei. American journal of human genetics, 57(5), 1143–1150.

16. Aviv, H., Khan, M. Y., Skurnick, J., Okuda, K., Kimura, M., Gardner, J., Priolo, L., & Aviv, A. (2001). Age dependent aneuploidy and telomere length of the human vascular endothelium. Atherosclerosis, 159(2), 281–287. https://doi.org/10.1016/s0021-9150(01)00506-8

17. Bloom, S. I., Liu, Y., Tucker, J. R., Islam, M. T., Machin, D. R., Abdeahad, H., Thomas, T. G., Bramwell, R. C., Lesniewski, L. A., & Donato, A. J. (2023). Endothelial cell telomere dysfunction induces senescence and results in vascular and metabolic impairments. *Aging cell*, *22*(8), e13875. https://doi.org/10.1111/acel.13875

18. Raj Bhayadia, Bernhard M. W. Schmidt, Anette Melk, Meike Hömme, Senescence-Induced Oxidative Stress Causes Endothelial Dysfunction, The Journals of Gerontology: Series A, Volume 71, Issue 2, February 2016, Pages 161–169, https://doi.org/10.1093/gerona/glv008

19. Levine, M. S., & Holland, A. J. (2018). The impact of mitotic errors on cell proliferation and tumorigenesis. Genes & development, 32(9-10), 620–638. https://doi.org/10.1101/gad.314351.118

20. Donato, A. J., Morgan, R. G., Walker, A. E., & Lesniewski, L. A. (2015). Cellular and molecular biology of aging endothelial cells. Journal of molecular and cellular cardiology, 89(Pt B), 122–135. https://doi.org/10.1016/j.yjmcc.2015.01.021

21. Han, Y., & Kim, S. Y. (2023). Endothelial senescence in vascular diseases: current understanding and future opportunities in senotherapeutics. *Experimental & Molecular Medicine*, *55*(1), 1-12. https://doi.org/10.1038/s12276-022-00906-w

22. Donato, A. J., Machin, D. R., & Lesniewski, L. A. (2018). Mechanisms of Dysfunction in the Aging Vasculature and Role in Age-Related Disease. *Circulation research*, *123*(7), 825–848. https://doi.org/10.1161/CIRCRESAHA.118.312563

23. Lin P. P. (2020). Aneuploid Circulating Tumor-Derived Endothelial Cell (CTEC): A Novel Versatile Player in Tumor Neovascularization and Cancer Metastasis. Cells, 9(6), 1539. https://doi.org/10.3390/cells9061539

24. Maishi, N., Ohba, Y., Akiyama, K. et al. Tumour endothelial cells in high metastatic tumours promote metastasis via epigenetic dysregulation of biglycan. Sci Rep 6, 28039 (2016). https://doi.org/10.1038/srep28039

25. Burssed, B., Zamariolli, M., Bellucco, F. T., & Melaragno, M. I. (2022). Mechanisms of structural chromosomal rearrangement formation. *Molecular cytogenetics*, *15*(1), 23. https://doi.org/10.1186/s13039-022-00600-6

26. Burgess, R. C., Misteli, T., & Oberdoerffer, P. (2012). DNA damage, chromatin, and transcription: the trinity of aging. Current opinion in cell biology, 24(6), 724–730. https://doi.org/10.1016/j.ceb.2012.07.005

27. Krumm, A., & Duan, Z. (2019). Understanding the 3D genome: Emerging impacts on human disease. *Seminars in cell & developmental biology*, *90*, 62–77. https://doi.org/10.1016/j.semcdb.2018.07.004

28. Jacobs, K. B., Yeager, M., Zhou, W., Wacholder, S., Wang, Z., Rodriguez-Santiago, B., Hutchinson, A., Deng, X., Liu, C., Horner, M. J., Cullen, M., Epstein, C. G., Burdett, L., Dean, M. C., Chatterjee, N., Sampson, J., Chung, C. C., Kovaks, J., Gapstur, S. M., Stevens, V. L., … Chanock, S. J. (2012). Detectable clonal mosaicism and its relationship to aging and cancer. *Nature genetics*, *44*(6), 651–658. https://doi.org/10.1038/ng.2270

29. Laurie, C. C., Laurie, C. A., Rice, K., Doheny, K. F., Zelnick, L. R., McHugh, C. P., Ling, H., Hetrick, K. N., Pugh, E. W., Amos, C., Wei, Q., Wang, L. E., Lee, J. E., Barnes, K. C., Hansel, N. N., Mathias, R., Daley, D., Beaty, T. H., Scott, A. F., Ruczinski, I., … Weir, B. S. (2012). Detectable clonal mosaicism from birth to old age and its relationship to cancer. *Nature genetics*, *44*(6), 642–650. https://doi.org/10.1038/ng.2271

30. Wood, J. G., & Helfand, S. L. (2013). Chromatin structure and transposable elements in organismal aging. Frontiers in genetics, 4, 274. https://doi.org/10.3389/fgene.2013.00274

31. Wood, J. G., Hillenmeyer, S., Lawrence, C., Chang, C., Hosier, S., Lightfoot, W., Mukherjee, E., Jiang, N., Schorl, C., Brodsky, A. S., Neretti, N., & Helfand, S. L. (2010). Chromatin remodeling in the aging genome of Drosophila. Aging cell, 9(6), 971–978. https://doi.org/10.1111/j.1474-9726.2010.00624.x

32. Divyaa Srinivasan, Tarak Shisode, Jatin Shrinet, Peter Fraser; Chromosome organization through the cell cycle at a glance. J Cell Sci 15 May 2022; 135 (10): jcs244004. doi: https://doi.org/10.1242/jcs.244004

33. Hua LL, Casas CJ, Mikawa T. Mitotic Antipairing of Homologous Chromosomes. Results and Problems in Cell Differentiation. 2022 ;70:191-220. DOI: 10.1007/978-3-031-06573-6_6. PMID: 36348108; PMCID: PMC9731508.

34. Srinivasan, D., Shisode, T., Shrinet, J., & Fraser, P. (2022). Chromosome organization through the cell cycle at a glance. *Journal of cell science*, *135*(10), jcs244004. https://doi.org/10.1242/jcs.244004

35. Alavattam, K. G., Mitzelfelt, K. A., Bonora, G., Fields, P. A., Yang, X., Chiu, H. S., Pabon, L., Bertero, A., Palpant, N. J., Noble, W. S., & Murry, C. E. (2023). Dynamic chromatin organization and regulatory interactions in human endothelial cell differentiation. *Stem cell reports*, *18*(1), 159–174. https://doi.org/10.1016/j.stemcr.2022.11.003

36. Hua LL, Mikawa T (2018). Mitotic anti-pairing of homologous and sex chromosomes via spatial restriction of two haploid sets. Proc. Natl. Acad. Sci. U.S.A. 115(52):E12235-E12244. (PMID:30530674; PMC6310853)

37. Cai, P., Casas, C. J., Quintero Plancarte, G., Mikawa, T., & Hua, L. L. (2025). Ipsilateral restriction of chromosome movement along a centrosome, and apical-basal axis during the cell cycle. *Chromosome Research*, *33*(1), 1-21.

38. Koeman, Julie M et al. “Somatic pairing of chromosome 19 in renal oncocytoma is associated with deregulated EGLN2-mediated [corrected] oxygen-sensing response.” *PLoS genetics* vol. 4,9 e1000176. 5 Sep. 2018, doi:10.1371/journal.pgen.1000176

39. Faruqi et al., S.A., Miller, R.C., Noumoff J.S. (1994). Somatic Pairing: AN Alternative for development of Cancer and other Hereditary Diseases. Cytologia. 59:439-444.

40. Atkin, N B, and Z Jackson. “Evidence for somatic pairing of chromosome 7 and 10 homologs in a follicular lymphoma.” *Cancer genetics and cytogenetics* vol. 89,2 (1996): 129-31. doi:10.1016/0165-4608(95)00360-6

41. Viti, Andrea et al. “A practical overview on probability distributions.” *Journal of thoracic disease* vol. 7,3 (2015): E7-E10. doi:10.3978/j.issn.2072-1439.2015.01.37

42. Muller, W A, and M A Gimbrone Jr. “Plasmalemmal proteins of cultured vascular endothelial cells exhibit apical-basal polarity: analysis by surface-selective iodination.” *The Journal of cell biology* vol. 103,6 Pt 1 (1986): 2389-402. doi:10.1083/jcb.103.6.2389

43. O'Toole, Eileen et al. “The role of γ-tubulin in centrosomal microtubule organization.” *PloS one* vol. 7,1 (2012): e29795. doi:10.1371/journal.pone.0029795

44. Zody, M. C., Garber, M., Adams, D. J., Sharpe, T., Harrow, J., Lupski, J. R., Nicholson, C., Searle, S. M., Wilming, L., Young, S. K., Abouelleil, A., Allen, N. R., Bi, W., Bloom, T., Borowsky, M. L., Bugalter, B. E., Butler, J., Chang, J. L., Chen, C. K., Cook, A., … Nusbaum, C. (2006). DNA sequence of human chromosome 17 and analysis of rearrangement in the human lineage. Nature, 440(7087), 1045–1049. https://doi.org/10.1038/nature04689

45. Kireeva, Natashe et al. “Visualization of early chromosome condensation: a hierarchical folding, axial glue model of chromosome structure.” *The Journal of cell biology* vol. 166,6 (2004): 775-85. doi:10.1083/jcb.200406049

46. Meaburn, K. J., Misteli, T., & Soutoglou, E. (2007). Spatial genome organization in the formation of chromosomal translocations. Seminars in cancer biology, 17(1), 80–90. https://doi.org/10.1016/j.semcancer.2006.10.008

47. Xu, X., Zhang, Y., & Li, M. (2020). NORs on human acrocentric chromosome p-arms are active by default and can associate with nucleoli independently of rDNA. Proceedings of the National Academy of Sciences, 117(19), 10352–10360. https://doi.org/10.1073/pnas.2001812117

48. Jiang, L., Wang, Y., & Zhang, L. (2018). Genetics of the human Y chromosome and its association with male infertility. *Reproductive Biology and Endocrinology, 16*(1), 1-10. https://doi.org/10.1186/s12958-018-0330-5

49. Cremer, M., Hase, J. V., Volm, T., Brero, A., Kreth, G., Walter, J., … Cremer, T. (2001). Non-random radial higher-order chromatin arrangements in nuclei of diploid human cells. Chromosome Research, 9(7), 541–567. https://doi.org/10.1023/A:1012495201697

50. Sun, H. B., Shen, J., & Yokota, H. (2000). Size-dependent positioning of human chromosomes in interphase nuclei. *Biophysical journal*, *79*(1), 184–190. https://doi.org/10.1016/S0006-3495(00)76282-5

51. Bolzer, A., Kreth, G., Solovei, I., Koehler, D., Saracoglu, K., Fauth, C., Müller, S., Eils, R., Cremer, C., & Speicher, M. R. (2005). Three-dimensional maps of all chromosomes in human male fibroblast nuclei and prometaphase rosettes. PLoS Biology, 3(5), 0826–0842. https://doi.org/10.1371/journal.pbio.0030142

52. Emmerich, P., Loos, P., Jauch, A., Hopman, A. H. N., Wiegant, J., Higgins, M. J., White, B. N., Van Der Ploeg, M., Cremer, C., & Cremer, T. (1989). Double in situ hybridization in combination with digital image analysis: A new approach to study interphase chromosome topography. Experimental Cell Research, 181(1), 126–140. https://doi.org/10.1016/0014-4827(89)90153-1

53. Weng, S., Stoner, S. A., & Zhang, D. E. (2016). Sex chromosome loss and the pseudoautosomal region genes in hematological malignancies. *Oncotarget*, *7*(44), 72356–72372. https://doi.org/10.18632/oncotarget.12050

54. Zhang, L. J., Shin, E. S., Yu, Z. X., & Li, S. B. (2007). Molecular genetic evidence of Y chromosome loss in male patients with hematological disorders. *Chinese medical journal*, *120*(22), 2002–2005.

55. Jin, Y., Mertens, F., Mandahl, N., Heim, S., Olegård, C., Wennerberg, J., Biörklund, A., & Mitelman, F. (1993). Chromosome abnormalities in eighty-three head and neck squamous cell carcinomas: influence of culture conditions on karyotypic pattern. *Cancer research*, *53*(9), 2140–2146.

56. Stone, J. F., & Sandberg, A. A. (1995). Sex chromosome aneuploidy and aging. *Mutation research*, *338*(1-6), 107–113. https://doi.org/10.1016/0921-8734(95)00016-y

57. Lewis et al., J P et al. “Somatic pairing of centromeres and short arms of chromosome 15 in the hematopoietic and lymphoid system.” *Human genetics* vol. 92,6 (1993): 577-82. doi:10.1007/BF00420942

58. Zhang, L et al. “Loss of chromosome 13 in cultured human vascular endothelial cells.” Experimental cell research vol. 260,2 (2000): 357-64. doi:10.1006/excr.2000.4997

59. Wiktor, A., Rybicki, B. A., Piao, Z. S., Shurafa, M., Barthel, B., Maeda, K., & Van Dyke, D. L. (2000). Clinical significance of Y chromosome loss in hematologic disease. *Genes, chromosomes & cancer*, *27*(1), 11–16.

60. Pierre, R. V., & Hoagland, H. C. (1972). Age-associated aneuploidy: loss of Y chromosome from human bone marrow cells with aging. *Cancer*, *30*(4), 889–894. https://doi.org/10.1002/1097-0142(197210)30:4%3C889::AID-CNCR2820300405%3E3.0.CO;2-1

61. Sakurai, M., & Sandberg, A. A. (1976). The chromosomes and causation of human cancer and leukemia. XVIII. The missing Y in acute myeloblastic leukemia (AML) and Ph1-positive chronic myelocytic leukemia (CML). *Cancer*, *38*(2), 762–769. https://doi.org/10.1002/1097-0142(197210)30:4%3C889::AID-CNCR2820300405%3E3.0.CO;2-1

62. Miyai, T., Maruyama, Y., Osakabe, Y., Nejima, R., Miyata, K., & Amano, S. (2008). Karyotype changes in cultured human corneal endothelial cells. *Molecular vision*, *14*, 942–950.

63. Aviv, H., Khan, M. Y., Skurnick, J., Okuda, K., Kimura, M., Gardner, J., Priolo, L., & Aviv, A. (2001). Age dependent aneuploidy and telomere length of the human vascular endothelium. *Atherosclerosis*, *159*(2), 281–287. https://doi.org/10.1016/s0021-9150(01)00506-8

64. Kimura, M., Cao, X., Patel, S., & Aviv, A. (2004). Survival advantage of cultured human vascular endothelial cells that lost chromosome 13. *Chromosoma*, *112*(7), 317–322. https://doi.org/10.1007/s00412-004-0276-6

65. Lezhava T. A. (1984). The activity of nucleolar organizer regions of human chromosomes in extreme old age. *Gerontology*, *30*(2), 94–99. https://doi.org/10.1159/000212614

66. Hamuro, J., Ueno, M., Toda, M., Sotozono, C., Montoya, M., & Kinoshita, S. (2016). Cultured Human Corneal Endothelial Cell Aneuploidy Dependence on the Presence of Heterogeneous Subpopulations With Distinct Differentiation Phenotypes. *Investigative ophthalmology & visual science*, *57*(10), 4385–4392. https://doi.org/10.1167/iovs.16-19771

67. Helena Mangs, A., & Morris, B. J. (2007). The Human Pseudoautosomal Region (PAR): Origin, Function and Future. Current genomics, 8(2), 129–136. https://doi.org/10.2174/138920207780368141

68. Nath, J et al. “Y chromosome aneuploidy, micronuclei, kinetochores and aging in men.” ‘*Chromosoma* vol. 103,10 (1995): 725-31. doi:10.1007/BF00344234

69. JACOBS, P., BRUNTON, M., COURT BROWN, W. *et al.* Change of Human Chromosome Count Distributions with Age: Evidence for a Sex Difference. *Nature* 197, 1080–1081 (1963). https://doi.org/10.1038/1971080a0

70. Gutiérrez-Hurtado, I. A., Sánchez-Méndez, A. D., Becerra-Loaiza, D. S., Rangel-Villalobos, H., Torres-Carrillo, N., Gallegos-Arreola, M. P., & Aguilar-Velázquez, J. A. (2024). Loss of the Y Chromosome: A Review of Molecular Mechanisms, Age Inference, and Implications for Men's Health. International journal of molecular sciences, 25(8), 4230. https://doi.org/10.3390/ijms25084230

71. Lau, S., Rangarajan, R., Krüger-Genge, A., Braune, S., Küpper, J. H., Lendlein, A., & Jung, F. (2020). Age-related morphology and function of human arterial endothelial cells. *Clinical hemorheology and microcirculation*, *74*(1), 93–107. https://doi.org/10.3233/CH-199238

Table

Table 1: Data Analysis of pooled HUVECs and individual HAECs patients

Human Umbilical Vein Endothelial Cells (HUVECs)	Chr. 1	Chr. 4	Chr. 13	Chr. 15	Chr. 17	Chr. 19	Chr. 21	Chr. 22	Chr. X	Chr. Y
Total neonatal samples (20 patients)	n=31 cells	n=28 cells	n=33 cells	n=41 cells	n=12 cells	n=35 cells	n=32 cells	n=22 cells	n=19 cells	n=16 cells
Human Aortic Endothelial Cells (HAECs)	Chr. 1	Chr. 4	Chr. 13	Chr. 15	Chr. 17	Chr. 19	Chr. 21	Chr.22	Chr. X	Chr. Y
Total adult samples (6 patients)	n=60 cells	n=50 cells	n=47 cells	n=50 cells	n=82 cells	n=38 cells	n=51 cells	n=52 cells	n= 86 cells	n=43 cells
Patient #1: 21 Year Old Male	n=7 cells	n=4 cells	N/A	N/A	N/A	N/A	N/A	n=6 cells	N/A	n= 16 cells
Patient #2: 36 Year Old Female	n=18 cells	n=10 cells	n=23 cells	n=25 cells	n=44 cells	n=8 cells	n=25 cells	n=1 cell	n= 37 cells	N/A
Patient #3: 50 Year Old Male	n=6 cells	n=1 cell	n=12 cells	N/A	N/A	n=4 cells	n=14 cells	n=8 cells	N/A	n= 8 cells
Patient #4: 50 Year Old Female	n=27 cells	n=30 cells	N/A	n=17 cells	n=5 cells	N/A	N/A	n=21 cells	n=38 cells	N/A
Patient #5: 50 Year Old Female	n=2 cells	n=5 cells	n=4 cells	N/A	n=12 cells	n=18 cells	n=3 cells	n=15 cells	n=11 cells	N/A
Patient #6: 68 Year Old Male	n=8 cells	N/A	n=8 cells	n=8 cells	n=21 cells	n=8 cells	n=9 cells	n=1 cell	N/A	n= 19 cells

Table 1: Data of pooled HUVECs and individual HAEC patients.
Data collected of pooled HUVECs (n=20 patients) and individual HAECs (n=6 individual patients) for chromosomes 1 (magenta), 4 (green), 13 (red), 15 (green), 17 (cyan), 19 (magenta), 21 (magenta), 22 (yellow), X (red), and Y (cyan).

Figures

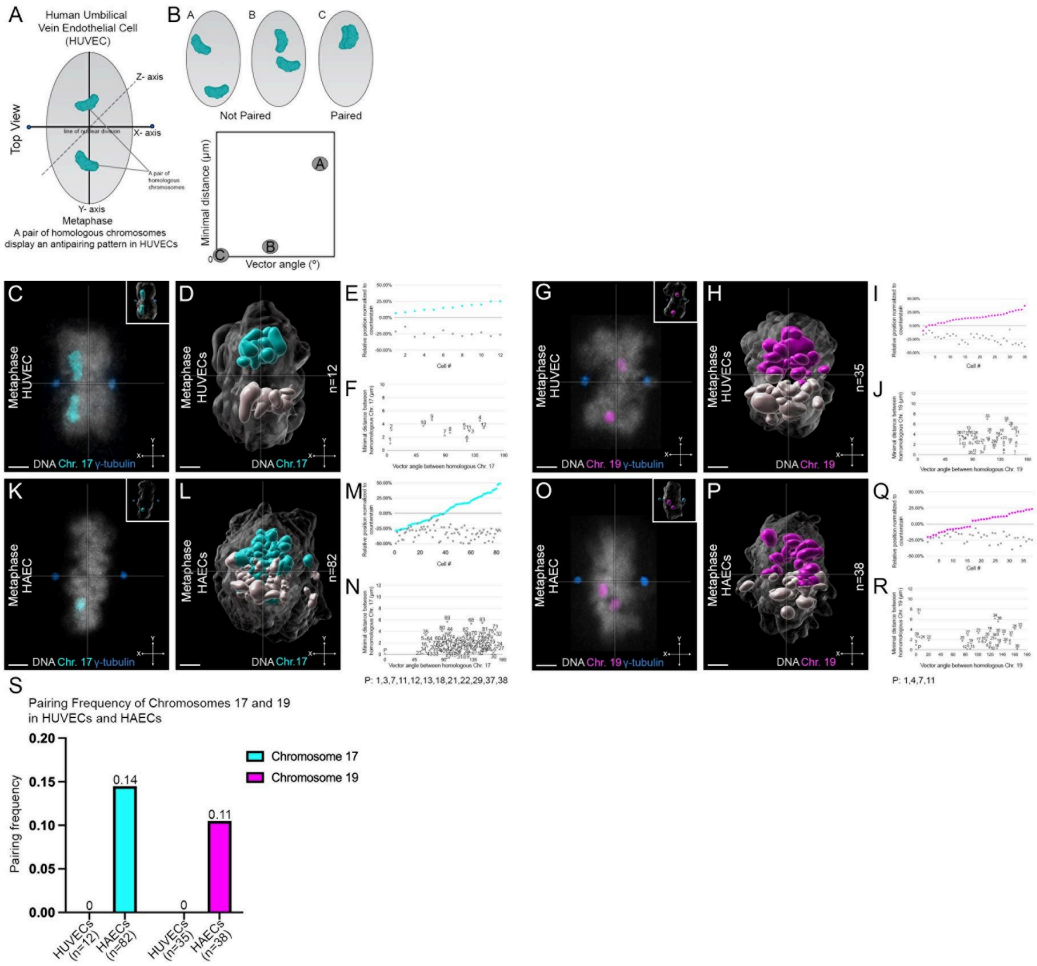

Figure 1: Homologous chromosome segregation is lost in small chromosomes 17, and 19 in adult HAECs.

(A) Schematic shows a pair of homologous chromosomes localize on opposite sides of the nuclear hemisphere for both autosomal, and sex chromosomes in neonatal human vein endothelial cells (HUVECs) (Hua and Mikawa 2018). **(B)** Pairing is defined as the distance between two homologous chromosomes to be at 0 µm and the vector angle between the two homologous chromosomes at 0°. Different scenarios of not paired (a,b) vs paired (c) are shown. **(C)** Top view of optical sections of a HUVEC at metaphase stained for chromosomes 17 (cyan), γ-tubulin (blue), and counterstained for DNA (grey). Inset: 3D reconstruction of the optical sections. **(D)** A 3D overlay of chromosome 17 (cyan/grey) of multiple HUVECs at metaphase, where the homolog closest to the x-axis is colored (cyan), while its respective partner is in grey (n=12 cells). **(E)** Relative positions for each homolog of chromosome 17 (cyan/grey circles) when mapped to an axial coordinate system. **(F)** The distance and angular orientation of homologous chromosome 17 pairs with an average distance of 2.97 ± 1.07 µm SD and angular orientation of 92.5° ± 49.1°. *Note: Each numbered cell corresponds to the same cell number in the relative position normalized to the DNA counterstain (E).* **(G-J)** As in C-F, but of chromosome 19 (n=35 cells). The distance and angular orientation of chromosome 19 homologs with an average distance of 2.90 ± 1.74 µm SD and angular orientation of 114.2° ± 29.7°. **(K-N)** As in C-F, but of adult human aortic endothelial cells (HAECs) (n=4 individual

patients, n=82 cells) with an average distance of 1.66 ± 1.39 µm SD and angular orientation of 101.0° ± 51.2°. **(O-R)** As in G-J, but of HAECs. The distance and angular orientation of chromosome 19 homologs (n=4 individual patients, n=38 cells) with an average distance of 2.02 ± 1.79 µm SD and angular orientation of 93.8° ± 55.8° SD. **(S)** Pairing frequency graph showing the pairing of chromosomes 17 (cyan) and 19 (magenta) of HUVECs and HAECs. Scale bar: 2 µm.

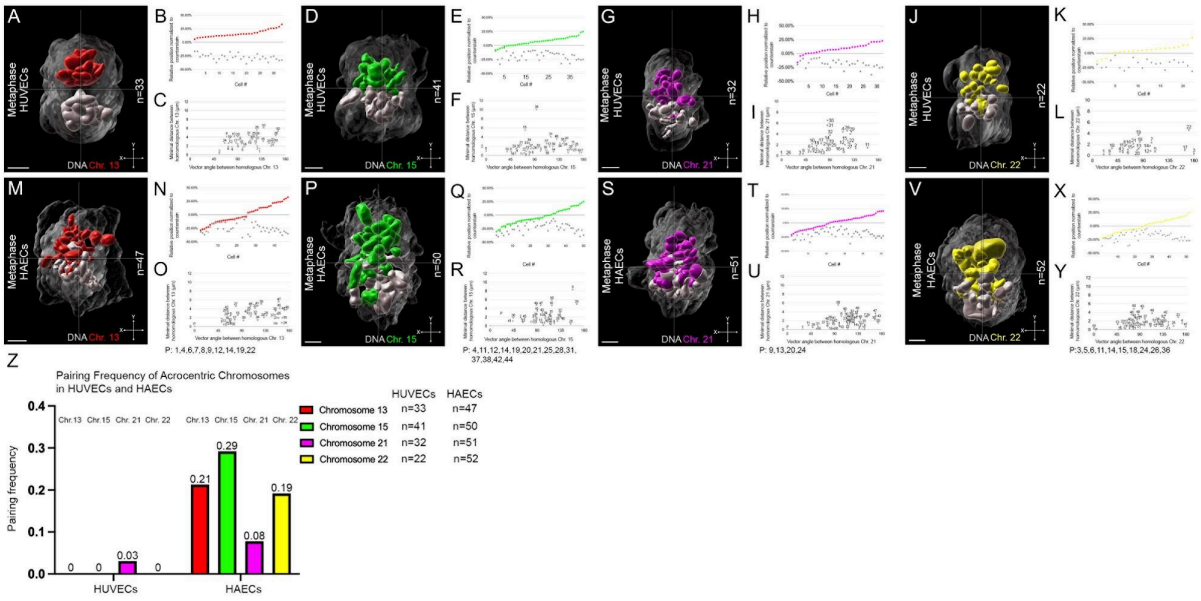

Figure 2: Homologous chromosome segregation is lost in acrocentric chromosomes 13, 15, 21, and 22 in adult HAECs.
(A) A 3D overlay of chromosomes 13 (red/grey) of multiple neonatal HUVECs at metaphase (n=33 cells). **(B)** Relative positions for each homolog of chromosome 13 (red/grey circles) when mapped to an axial coordinate system. **(C)** The distance and angular orientation of homologous chromosome 13 pairs with an average distance of 3.18 ± 1.27 µm SD and angular orientation of 111.2° ± 31.5° SD. *Note: Each cell is numbered as in Fig. 1.* **(D-F)** As in (A-C) but of homologous chromosome 15 (green/grey) (n=41 cells). The distance and angular orientation of chromosome 15 homologs with an average distance of 1.88 ± 1.71 µm SD and angular orientation of 101.9° ± 42.2° SD. **(G-I)** As in (A-C) but of chromosome 21 homologs (magenta/grey) (n=32 cells). The distance and angular orientation of chromosome 21 homologs with an average distance of 2.21 ± 1.58 µm SD and angular orientation of 87.7° ± 36.6°SD. **(J-L)** As in (A-C) but of chromosome 22 homologs (yellow/grey) (n=22 cells). The distance and angular orientation of chromosome 22 homologs with an average distance of 1.49 ± 1.08 µm SD and angular orientation of 83.4° ± 43.2°. **(M-O)** As in (A-C), but of adult HAECs (n=4 individual patients, n=47 cells) with an average distance of 2.05 ± 1.66 µm SD and angular orientation of 87.1° ± 58.2°SD. **(P-R)** As in (D-F), but of adult HAECs (n=3 individual patients, n=50 cells). The distance and angular orientation of chromosome 15 homologs with an average distance of 1.67 ± 1.85 µm SD and angular orientation of 73.5° ± 53.7° SD. **(S-U)** As in (G-I), but of adult HAECs (n=4 individual patients, n=51 cells) with an average distance of 1.81 ± 1.34 µm SD and angular orientation of 102.9° ± 45.0°. **(V-Y)** As in (J-L), but of adult HAECs (n=6 individual patients, n=52 cells). The distance and angular orientation of homologues of chromosome 22 with an average distance of 1.42 ± 1.26 µm SD and angular orientation of 81.2° ± 52.6°. **(Z)** Pairing frequency graph showing the pairing of chromosomes 13 (red), 15 (green), 21 (magenta), 22 (yellow) of HUVECs and HAECs. Scale bar: 2 µm.

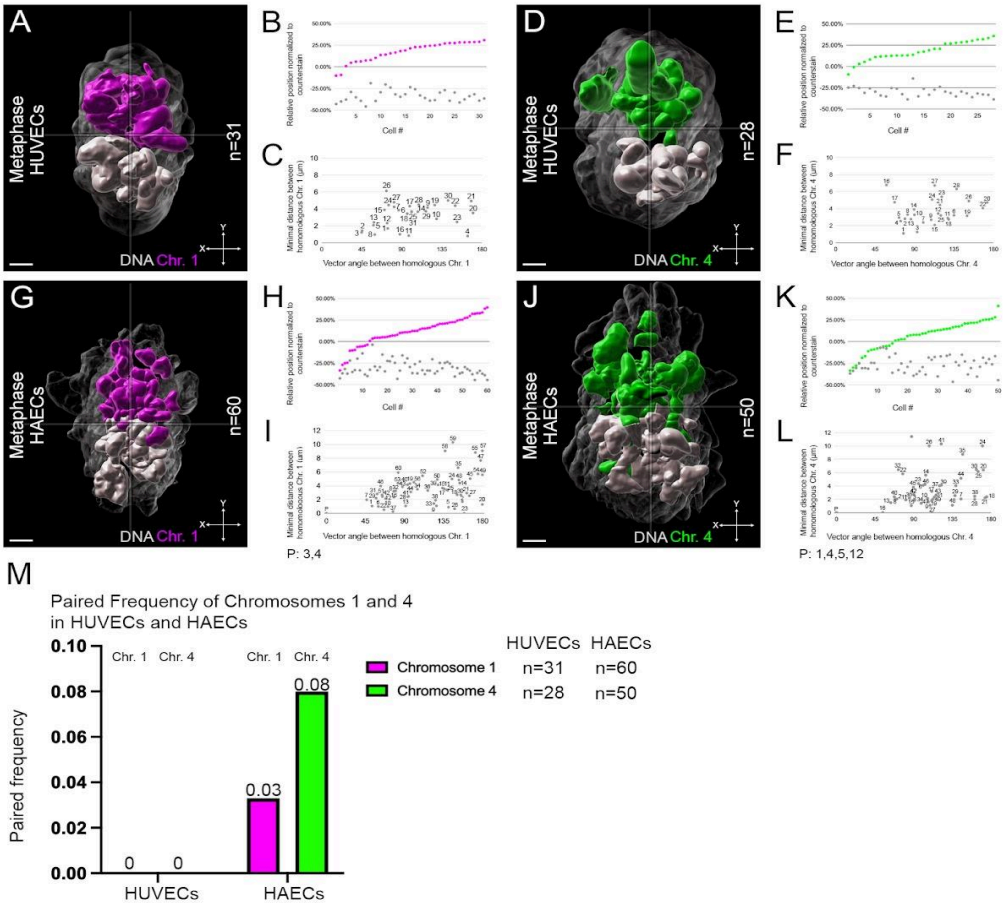

Figure 3: Fewer adult HAECs show loss of segregation for the larger chromosomes 1 and 4.

(A) A 3D overlay of chromosome 1 (magenta/grey) of multiple neonatal HUVECs at metaphase (n=31 cells). **(B)** Relative positions for each homolog of chromosome 1 (magenta/grey circles) when mapped to an axial coordinate system. **(C)** The distance and angular orientation for the chromosome 1 homologs with an average distance of 3.25 ± 1.45 µm SD and angular orientation of 100.6° ± 35.9°. *Note: Each cell is numbered as in Fig. 1.* **(D-F)** As in A-C, but of chromosome 4. Chromosome 4 homologs have an average distance of 3.66 ± 1.48 µm SD and angular orientation of 109.4° ± 30.4° (n=28 cells). **(G-I)** As in A-C, but of adult HAECs. The distance and angular orientation chromosome 1 homologs (n=6 individual patients, n=60 cells) with an average distance of 3.25 ± 1.44 µm SD and angular orientation of 100.6° ± 35.9°. **(J-L)** As in D-F, but of adult HAECs (n=5 individual patients, n=50 cells). The distance and angular orientation chromosome 4 homologs with an average distance of 3.39 ± 2.34 µm SD and angular orientation of 112.9° ± 44.7°. **(M)** Pairing frequency graph of chromosome 1 (magenta) and chromosome 4 (green) for both HUVECs and HAECs. Scale bar: 2 µm.

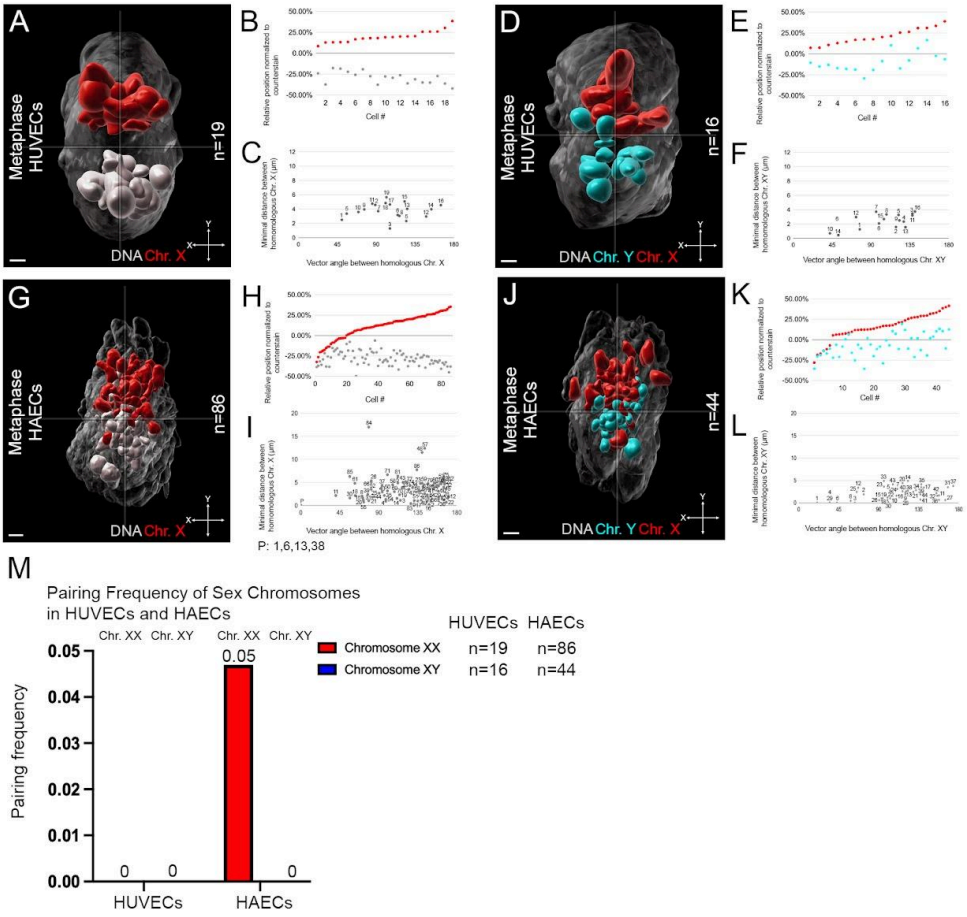

Figure 4: Fewer female adult HAECs exhibit loss of XX chromosome spatial segregation and abnormal pairing, while in male adult HAECs, the XY sex chromosomes lose segregation but do not pair.

(A) A 3D overlay of chromosome XX (red/grey) of multiple neonatal HUVECs at metaphase (n=19 cells). **(B)** Relative positions for each homolog of chromosome X (red/grey circles) when mapped to an axial coordinate system. **(C)** The distance and angular orientation of chromosome X homologs with an average distance of 3.78 ± 1.08 μm SD and angular orientation of 105.6° ± 31.2°. *Note: Each cell is numbered, as in Fig. 1.* **(D-F)** As in A-C, but of XY (red/cyan) sex chromosomes (n=16 cells) with an average distance of 2.42 ± 1.06 μm SD and angular orientation of 105.7° ± 30.6°. **(G-I)** Same as A-C, but of female-derived HAECs (n=3 individual patients, n=86 cells). The distance and angular orientation of chromosome X homologs with an average distance of 3.38 ± 2.72 μm SD and angular orientation of 116.9° ± 42.0°. **(J-L)** As in D-F, but of multiple male-derived HAECs (n=3 male patients, n=44 cells) with an average distance of 2.04 ± 1.44 μm SD and angular orientation of 108.9° ± 37.5°. **(K)** Pairing frequency graph of chromosome XX (red) and chromosome XY (cyan) of HUVECs and HAECs. Scale bar: 2 μm.

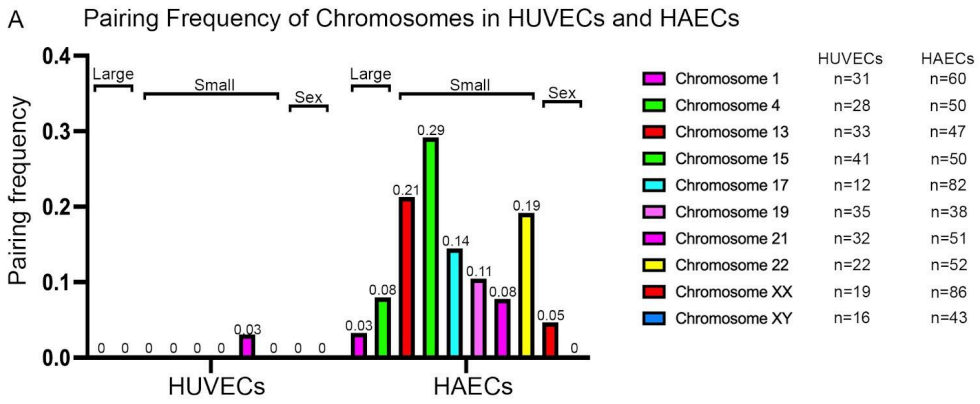

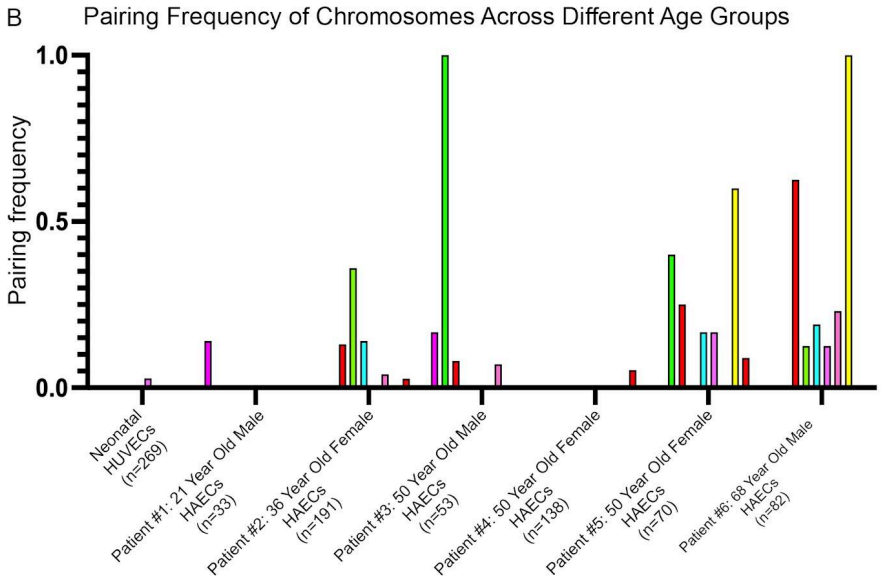

C

	Pairing frequency	Total number of cells
HUVECs Neonatal	0.40%	269
HAECs 21 Year Old	6.10%	33
HAECs 36 Year Old	10.50%	191
HAECs 50 Year Old	9.60%	261
HAECs 68 Year Old	20.70%	82

Figure 5: Pairing frequency analysis shows smaller chromosomes have an increase in abnormal pairing as compared to larger chromosomes in adult HAECs, with a trend of increased susceptibility of pairing throughout age.
(A) Chart representing pairing frequencies of HUVECs and HAECs across chromosomes 1 (magenta), 4 (green), 13 (red), 15 (green), 17 (cyan), 19 (magenta), 21 (magenta), (yellow), XX (red), and XY (blue). **(B)** Chart of pairing frequency of chromosomes across different age groups. **(C)** Table of pairing frequency percentage and sample sizes of analyzed cells across different age groups.

Supplemental figure 1: Characterizing the centrosome axis and center of chromosomal mass in HUVECs and HAECs.
(A) A metaphase HUVEC stained for γ-tubulin antibody (blue), and DNA (DAPI, grey). Yellow dot represents the center of mass of the DAPI stained chromosomal mass. Boxed region shows the x-, or centrosome axis. **(A')** Zoom in view of the boxed region in (A). Boundary zone (red line) is determined by measuring the distance between the chromosomal center of mass (yellow dot) and the centrosome axis (white dotted line). The distance between the centrosome axis (line connecting the centrosomes) and the chromosomal center of mass on average is ± 0.5 μm. Thus, a 1 μm width bounding box region of DAPI staining overlapping the chromosomal center of mass was determined as the "boundary zone" as previously described (Cai et al. 2025). **(B, B')** Same as (A, A'), but of HAECs. The average distance between the centrosome axis and the chromosomal center of mass is ± 0.45 μm. Therefore the boundary region is 0.90 μm for HAECs. Note: For chromosome painting analysis, if the center of mass of an individual homolog was ± 0.5 μm for HUVECs and ± 0.45 for HAECs from the chromosomal center of mass along the x-axis, these cells were not used in our analysis as they were uninterpretable. For instance, out of 66 total cells, 6 cells exhibited homologous chromosome 1 in this boundary region, rendering the data uninterpretable (n=6/66 cells for chromosome 1). Scale bar: 2 μm.

Supplemental figure 2: Generation of a 3D overlay and analysis.
(A) Top view of the confocal staining at 63x magnification of HUVECs at interphase and metaphase stains for DNA (grey), γ-tubulin (blue), and chromosome 19 (magenta). Boxed region shows a mitotic cell. **(A')** As in (A), but a zoom in of the boxed region in (A) showing segregation of homologous chromosome 19. Center of the chromosomal mass (yellow dot) and centrosomes (blue dot) are aligned along the centrosome axis. Center of mass for each chromosome 19 is also shown (magenta dot). **(A")** A 3D reconstruction of optical confocal sections in (A'). **(A'")** To differentiate between each homologous chromosome, the one homolog that is closest to the x-, or centrosome, axis is designated in color (magenta), while its respective homolog is in grey. **(B)** Generation of a 3D overlay to determine if each pair of homologous chromosomes are spatially segregated from one another. Individual mitotic cells overlaid using the centrosome axis as previously described (Hua and Mikawa 2018). For each metaphase cell, we determined if they were spatially segregated by using the centrosome axis. If the homologous chromosomes are located on opposite sides, it indicates spatial segregation of the homologs. In contrast, if both homologous chromosomes are positioned on the same side along the centrosome axis, it signifies a loss of segregation. Scale bars: 10, 2 μm.

Supplemental Video 1: Homologous segregation is lost in acrocentric chromosome 13 in adult HAECs as compared to neonatal HUVECs.
Video of Whole Chromosome Painting of chromosome 13 and 3D overlays for HUVECs (top panels), and HAECs (bottom panels) rotating 360º counter-clockwise along the y-axis staining for chromosome 13 (red), and DNA (SYTOX, grey) for whole chromosome painting, and chromosome 13 surfaces (red/grey) for overlays. Scale bar: 3 μm.